IDE∆L®

Assignment of Coherence Features in NMR *q*-Space Plots to Particular Diffusion Modes in Erythrocyte Suspensions

Allan M. Torres, Andrew T. Taurins, David G. Regan, Bogdan E. Chapman, and Philip W. Kuchel[1]

Department of Biochemistry, University of Sydney, Sydney, New South Wales, 2006, Australia

NMR *q*-space plots derived from water diffusing inside and around erythrocytes in a suspension display reproducible and characteristic coherence features. The aim of the present work was to determine which water population gives rise to the respective features. The central experimental strategy was to use choline and choline phosphate which are virtually membrane impermeant on the time scale of the experiment; the former was incorporated into erythrocytes by a lysis-resealing method and the latter was simply added to the suspensions. Dimethyl sulfoxide, which readily but more slowly exchanges across the cell membranes than water, also yielded *q*-space plots which were similar to those of water, but the differences were able to be accounted for on the basis of its slower transmembrane exchange rate. Random walk simulations using a Monte Carlo procedure, together with a model of an array of biconcave discocytes, helped verify the interpretations of the assignment of the features of the plots to molecules diffusing in the two regions. In addition, the simulations revealed how the presence or absence of transmembrane exchange affects the form of *q*-space plots.   © 1999 Academic Press

Key Words: diffusion diffraction; NMR *q*-space; erythrocytes; random walk simulation; Monte Carlo.

INTRODUCTION

When the pulsed field gradient spin-echo (PFGSE) experiment is carried out on a suspension of diamagnetic erythrocytes, the plot of the logarithm of the normalized signal intensity, $\log_{10}(E[q, \Delta])$, *versus* the scaled magnitude of the gradient pulses q ($q = (2\pi)^{-1}\gamma g \delta$, where γ is the nuclear magnetogyric ratio, g is the magnitude of the field gradient pulses, and δ is the duration of each of the gradient pulses) displays "coherence" peaks (*1, 2*). The analogy between *q*-space plots derived from PFGSE experiments and diffraction patterns of physical optics was an important insight presented in 1990 (*3*). The experiment employing the ^{1}H NMR water signal has been shown to be capable of characterizing erythrocyte sizes and shapes in normal and disease states. Thus *q*-space analysis of erythrocyte suspensions is potentially useful as a diagnostic tool in hematology since it provides relatively unbiased estimates of population-mean cell dimensions and shapes in a sample (*2*).

Figure 1 shows a typical *q*-space plot of the water signal from a 0.30-hematocrit (Ht, volume fraction of the sample that is cells) suspension of metabolically active human erythrocytes. It is evident that the plot is characterized by a monotonic decline that is "embellished" with an inflection and several maxima and minima. These reproducible features in the declining curve provide more "specificity" in the subsequent estimates of lengths and distances than are typically available from multiple exponential analysis, or interpretation of the Gaussian-like curves that arise, for example, from yeast cells because of their size heterogeneity (*3*). From earlier experimental and theoretical work on randomly packed beds of polymer spheres (*4–6*) and glass spheres (*7*), it was predicted that some of the coherence features in *q*-space plots from erythrocyte suspensions would arise from water diffusing in the interstices between the cells. This coherence effect has been interpreted physically by using a simplified model referred to as "pore-hopping," and it bears an analogy with the two-slit interference experiment of physical optics (*8*). On the other hand, theoretical consideration has been given to spins constrained to move inside isolated (*not* interconnected) lacunae. These systems also display coherences in *q*-space plots, but the physical interpretation is that this is analogous to the single-slit diffraction effect of optics (*3, 9–11*). These two simple analogies with coherences in optics apply strictly only when the PFGSE experiment is carried out with the duration of the gradient pulses, δ, being negligible relative to the time interval, Δ, between them [viz., the short gradient pulse (SGP) approximation]. Also, the time over which the diffusion is measured, Δ, must be sufficiently large to ensure multiple interactions of the spins with the limiting barriers that are separated by the distance a; specifically, $\Delta \gg a^2/2D$, where D is the diffusion coefficient. Under these conditions the NMR signal intensity, $E[q, \Delta]$, is the power 2 spectrum (Fourier transform) of the autocorrelation function of the diffusion-restricting compartment(s) (*3, 9, 12, 13*).

Thus, since water is diffusing both inside and outside cells in a suspension, a *q*-space plot will be the superposi-

[1] To whom correspondence should be addressed. Fax: (+61-2) 9351 4726. E-mail: p.kuchel@biochem.usyd.edu.au.

AP

tion of the interference and diffraction effects noted above. In addition, in a cell suspension, exchange of water across the membranes will lead to a "mixing" of the two effects that will complicate the interpretation of the data. On the other hand, because the effects are mixed this might form the basis of a new means of measuring the rate of exchange across the membrane. Indeed, in a recent theoretical study of spin exchange out of spheres, it was shown that the positions of minima in q-space plots move to larger q values if the membrane permeability is increased (14). This phenomenon was observed experimentally in the earlier q-space study of human erythrocytes (1).

Therefore, the aim of the present work was to assign the various features of q-space plots from water, and other molecules, in erythrocyte suspensions to diffusing populations inside and outside the cells. We used molecular species, in addition to water, that were confined to either the outside or the inside of the cells, hence allowing separation of the interference and diffraction effects, and also eliminating the mixing of them due to transmembrane exchange. In our earlier studies (1, 2), we attributed the first diffraction peak, which appears as a "shoulder" near $q \sim 1.0 \times 10^5$ m^{-1}, to the pore-hopping phenomenon; this was verified in a more direct way in the present work. This interference peak was found to be more pronounced in lower hematocrit samples (Ht < 0.50) in which the relative amount of extracellular water was significantly higher. The second peak with $q_{max} \sim 2.2 \times 10^5$ m^{-1}, on the other hand, was ascribed to water diffusing inside the cells.

The reciprocal of the q position of the diffusion-interference *maximum* is inversely related to the mean distance between the interstitial water-filled cavities that exist between the cells in the suspension. These cavities are often referred to as "pores." The q positions of the diffusion-diffraction *minima* (q_{min}) are inversely related to the main dimension of the intracellular compartment, viewed in the direction of the field gradient pulses. Exact mathematical expressions derived with the SGP approximation, which relate signal intensity $E[q, \Delta]$ with the dimensions of simple compartments, have been presented by Callaghan; these include expressions for spherical, planar, and cylindrical lacunae (10). Such expressions do not exist for the biconcave disc of the mammalian erythrocyte, but numerical calculations using the expression for a discocyte (15) were done in the course of the present work (see Discussion).

It is also important to note that the rationale behind the peak assignments in the q-space plots from erythrocyte suspensions was based primarily on known erythrocyte dimensions from studies using microscopy (1, 2). No experimental results until now have been shown to separate and convincingly identify the two types of coherence peaks. Therefore, it was considered important to study each type of curve separated from the other.

MATERIALS AND METHODS

Sample Preparation

Blood was obtained from healthy human donors by venipuncture in the cubital fossa. The cells were centrifugally washed ($3000 \times g$, 5 min) three times in cold saline solution (154 mM NaCl, 10 mM glucose, pH 7.4, 290 mOsmol kg^{-1}, 4°C) and the buffy coat was removed by aspiration. Bubbling with CO was performed prior to the second wash in order to transform the hemoglobin into a stable low-spin diamagnetic state. All solutions used in the sample preparation contained 10 mM glucose. Samples for NMR studies were dispensed in two ways depending on the amount of sample: for small samples, $\sim$180 μL of cell suspension was dispensed into 5-mm-o.d. susceptibility-matched microtubes (BMS-005B, Shigemi, Tokyo, Japan). For larger samples, $\sim$600 μL of cell suspension was dispensed into a flat-bottom Wilmad insert tube made to go inside a 10-mm NMR tube (516-I-10, Wilmad, Buena, NJ). A Teflon vortex plug was inserted onto the top of the sample and the insert tube was in turn placed in the 10-mm-o.d. tube containing $\sim$1.0 mL CCl_4. The latter was used to avoid air–glass interfaces near the cell sample and thus minimized static local magnetic field gradients due to large differences in magnetic susceptibility.

Choline loading of the cells was achieved as follows by hypotonic hemolysis and resealing: 10 mL of washed cell pellet was mixed with 90 mL of hypotonic choline solution (45 mM choline chloride, 5 mM sodium phosphate buffer, pH 7.2) so that the final osmolality was $\sim$130 mOsmol kg^{-1}. This resulted in breaching the cell membranes, thus allowing choline to enter the cells. The suspension was incubated for 5 min at 0°C, and then 100 mL of hypertonic "resealing" solution (206 mM LiCl, 10 mM $CaCl_2$, 8 mM $MgCl_2$, 4 mM adenosine, 480 mOsmol kg^{-1}) was added. The resulting mixture was allowed to stand at 37°C for 1 h. Lithium chloride was used in the incubation medium to restrict the efflux of intracellular choline (16) while $CaCl_2$ and $MgCl_2$ were added to maintain the biconcave shape of the cells. However, light microscopy showed that the mean cell shape after resealing was not perfectly biconcave but either spherical or stomatocytic. Approximately 1 mL of the pelleted resealed cells was centrifugally washed three times with ^2H_2O containing 154 mM lithium chloride. The hematocrit of the resulting suspension was adjusted, as required, prior to the NMR experiment.

The introduction of choline phosphate and dimethyl sulfoxide (DMSO) into the cell suspensions was much simpler. This was done by centrifugally washing 1 mL of pelleted cells three times with 2 mL of the requisite solutions constituted in ^2H_2O. The solutions that were used were 72.5 mM choline phosphate, and 4–7% (v/v) DMSO. The phosphate group on choline phosphate prevents this compound from entering the cells while DMSO is known to enter the cells freely.

NMR Spectroscopy

PFGSE NMR experiments were performed on a Bruker AMX 400 wide-bore spectrometer equipped with a gradient probe capable of delivering a maximum gradient of ~10 T m^{-1} in the direction of $\mathbf{B}_0$. In all experiments, the standard PFGSE pulse sequence and phase cycles were used (1, 2). The probe temperature was set to 298 K. In a typical experiment, the duration of the $\pi/2$ pulse was 22 μs; that of the two gradient pulses, δ, was 2 ms; the time interval between the gradient pulses was 20 or 40 ms; the relaxation delay between transients was 3 s; and the number of transients per spectrum was 16 or 32. The field gradient was incremented in 32 or 96 steps to obtain a maximum value of ~9.6 Tm^{-1}.

The acquired data consisted of 1k of complex points spanning a spectral width of 1 or 2 kHz. No zero-filling of the data was used, and a line-broadening factor of 5–20 Hz was used with exponential multiplication of the data prior to its Fourier transformation. A Matlab program (1) was used to process and analyze the data; the relevant spectral peaks were automatically integrated and scaled to the largest peak in the series by this program.

Monte Carlo Simulations

Diffusion in the context of a PFGSE experiment was simulated by performing a three-dimensional random walk for an ensemble of noninteracting point molecules (water). This so-called Monte Carlo method followed procedures described previously for simulating q-space plots for samples composed of molecules diffusing in restricting geometries (17). Various new algorithms were designed and verified using *Mathematica* (18) to account for the particular geometry describing a biconcave disc. The simulation code was written in "C", and simulations were executed on either a Silicon Graphics workstation or a Pentium PC.

Simulation parameters were chosen to mimic as closely as possible a sample of erythrocytes at a packing density of 0.50 in isotonic solution. The main cell diameter was 8 μm, maximum thickness 2.12 μm, and thickness at the central "dimple" 1 μm, yielding a cell volume of 8.6×10^{-17} m^3. Each cell was assumed to occupy the center of a hexagonal prism, and periodic boundary conditions were applied, thus simplifying the study to a single "reference cell" centered on the Cartesian origin (17, 19). The diffusion coefficient both inside and outside the cells was set to the same value of 2.0×10^{-9} m^2 s^{-1}. (The same value was used to minimize the number of different parameter values employed in the simulations.) In real cellular systems these values differ, but since the diffusion time was chosen to be relatively long, the condition $\Delta \gg a^2/2D$ would still have been met even if the diffusion coefficient for inside the cells was less than half of that for the molecules outside. The simulated field gradient was incremented in 96 steps, from an initial value of 0.0 to a maximum of 9.41 T m^{-1}. The set of simulated echo intensities for all gradients in any one simula-
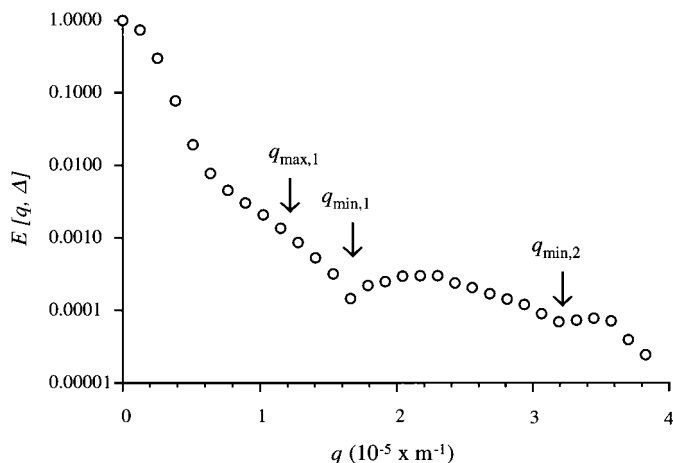

FIG. 1. ^{1}H NMR q-space plot of water in a suspension of fresh human erythrocytes with a hematocrit (Ht, fraction of the sample volume that is cells) of 0.30, at 298 K. The field gradient **g,** for this and all other experiments reported here, was applied in the direction of $\mathbf{B}_0$, namely the z axis. The assignments of diffusion modes to the various features of the curves are extracellular diffusion-interference ("pore-hopping") shoulder at $q_{max,1}$ and intracellular diffusion-diffraction minima at $q_{min,1}$ and $q_{min,2}$. The q positions of the interference and diffraction features are inversely related to the mean cell diameter, bearing in mind that the cells would have been aligned with their disc planes parallel to $\mathbf{B}_0$ (1).

tion was normalized to the maximum echo intensity produced when the gradient was zero. An "ensemble" consisted of 10×10^6 point molecules whose individual trajectories were studied. Each point molecule was assigned a random starting point and performed a random walk trajectory during the total diffusion time given by Δ (20 ms) + δ (2ms). During this time the molecule performed 3300 three-dimensional random jumps of length 28.28 μm, as determined by the Einstein equation for self-diffusion in *each* of the three dimensions, namely jump length = (2 D jump time)$^{1/2}$ (17, 19). The membrane transition probability was determined by trial simulations to ensure that the mean residence time for any point molecule inside the biconcave disc would be of the order of ~10 ms, in accordance with experimental values (20). The accumulated phase shifts of the magnetization (dipole moment per unit volume) for all point molecules, during the total diffusion time, were summed and averaged, and the echo intensity was then calculated for all gradient values and stored in an array. From this array of values the q-space plot was generated.

RESULTS

q-Space Plots from [1]H$_2$O in Suspensions of Erythrocytes

Figure 1 shows a typical ^{1}H NMR q-space plot obtained from the signal of water diffusing in a slightly hypotonic suspension of metabolically active human erythrocytes. The fact that the curve is not "monotonically strictly decreasing" is evident. The features of the curve are similar to those reported
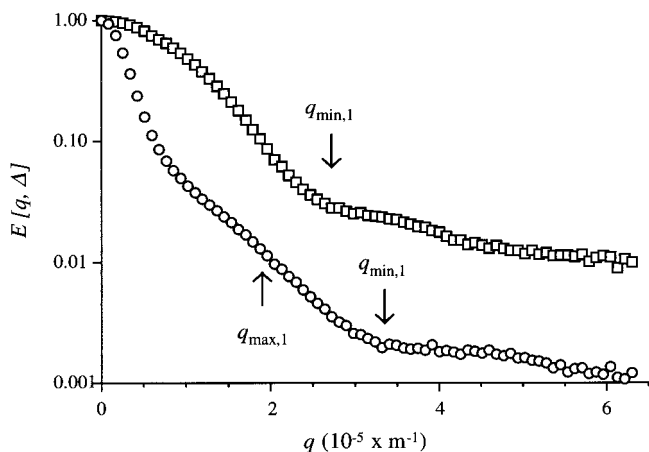
FIG. 2. ^{1}H NMR q-space plots of water ($\bigcirc$) and choline ($\square$) in a 0.70-Ht suspension of resealed erythrocytes loaded with choline, at 298 K. The water curve is very different from that in Fig. 1 because the resealed cells were no longer biconcave discs but rather were a mixture of stomatocytes and spherocytes. The minima in the choline curve resulted from intracellular diffusion diffraction only. The difference between the two plots is due to the absence of extracellular interference diffraction (pore hopping) and transmembrane exchange, with the choline.

FIG. 3. High-resolution ^{1}H NMR q-space plot of water in a 0.62-Ht suspension of spherical erythrocytes, at 310 K. The curve is notably similar to that of water in the suspension of resealed cells shown in Fig. 2.

previously (*1, 2*), but as a result of the higher values of field gradients now available, a higher order coherence was routinely observed. The shoulder centered at $\sim 1.2 \times 10^5$ m^{-1} (denoted $q_{max,1}$) was previously inferred to be due to pore hopping (*1, 2*); and the two minima at $\sim 1.6 \times 10^5$ and $\sim 3.2 \times 10^5$ m^{-1} are denoted $q_{min,1}$ and $q_{min,2}$, respectively. The physical bases of these three coherence features were addressed experimentally, as follows.

Choline and ^{1}H$_2$O q-Space Plots and Intracellular Diffusion Diffraction

Figure 2 shows the q-space plots for choline and water (residual ^{1}H^{2}HO) proton signals in a 0.70-Ht suspension of resealed erythrocytes. In the experiment, the duration of the spin-echo time, 2τ, was set to 40 ms compared with our commonly used value of 20–30 ms when water diffusion is studied (*1, 2*). This allowed for the fact that the diffusion coefficient of choline is significantly smaller than that of water. Comparison of the q-space plots from water in Figs. 1 and 2 clearly shows that the positions of the maxima and minima in the two curves were not the same. This difference implied an alteration of cell shape between the fresh erythrocytes used for Fig. 1 and the resealed cells used for Fig. 2. Light microscopic examination of the resealed cells showed that they were not strictly biconcave but rather were a mixture of distorted discs and spheres.

A typical q-space plot from water in a suspension of *spherical* erythrocytes, akin to those obtained in a previous study (*2*), is shown in Fig. 3. Examination of this plot reveals a distinct similarity to the profile obtained for water in the resealed cells
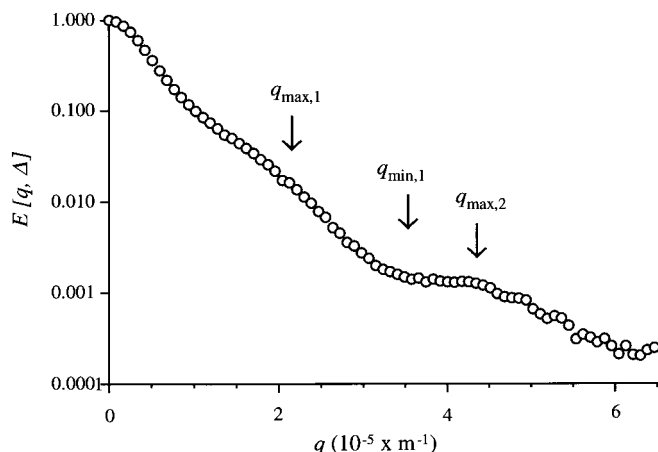
(Fig. 2). In both cases the first maximum (more correctly an "inflection," or a maximum in the first derivative) is at $\sim 2 \times 10^5$ m^{-1} ($q_{max,1}$) while the minimum ($q_{min,1}$) after the first maximum is at $\sim 3.4 \times 10^5$ m^{-1}. In the choline data $q_{min,1}$ is at $\sim 2.8 \times 10^5$ m^{-1} while the next maximum is at $\sim 3.5 \times 10^5$ m^{-1}. In our previous work (*2*) we attributed the first maximum in the water data (Fig. 3) to diffusion interference, while the second maximum (Fig. 3, $q_{max,2}$) was attributed to intracellular diffusion diffraction. On the other hand $q_{max,2}$ is not clearly delineated in Fig. 2 (see Discussion).

Choline Phosphate and ^{1}H$_2$O

Figure 4 shows the q-space plots of choline phosphate and water in a suspension of fresh red blood cells of Ht = 0.60.
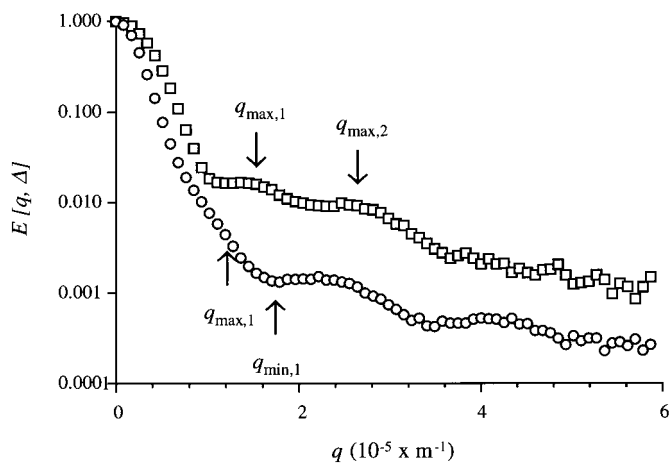

FIG. 4. ^{1}H NMR q-space plots of water ($\bigcirc$) and choline phosphate ($\square$) in a 0.60-Ht suspension of fresh erythrocytes, which had been washed in 72.5 mM choline phosphate, at 298 K. The peaks in the curve ($q_{max,1}$ and $q_{max,2}$), which are indicated by arrows, resulted from interference diffraction (pore hopping) only, since the choline phosphate was located exclusively extracellularly.
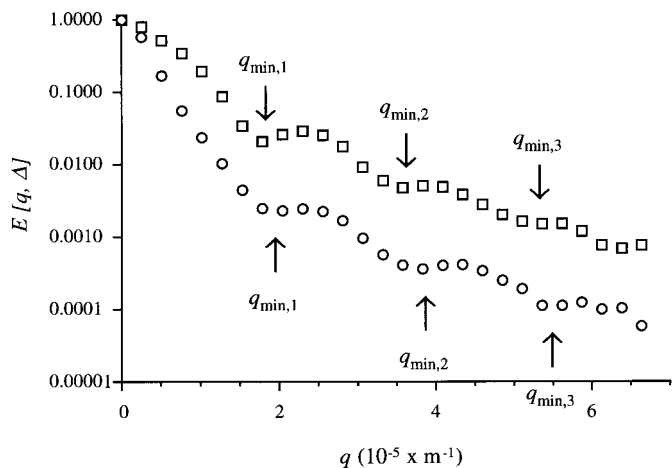
FIG. 5. ^{1}H NMR q-space plots of water (○) and DMSO (□) in a 0.60-Ht suspension of fresh erythrocytes that had been washed with 4% (v/v) DMSO, at 310 K. The DMSO curve is notably similar to the water curve, indicating that DMSO molecules were present inside and outside the cells. However, the signal attenuation of the DMSO was substantially less than that of water for a given q value.

Unlike the choline experiment (Fig. 2), in which the erythrocytes were primarily spherocytes (including some distorted discocytes), the cells in this case were all discocytes. This uniform cell shape was reflected in the form of the water q-space plot which was very similar to that from the metabolically active cells used for Fig. 1. For Fig. 4, the spin-echo time, 2τ, was set to 40 ms to enable a longer diffusion time, thus allowing for the smaller diffusion coefficient of choline phosphate. A large proportion of the water (60%) was located in the intracellular region (exchange notwithstanding) but the choline phosphate was only in the extracellular region; hence its diffusion would have been less restricted than if it were inside the cells. The apparent diffusion coefficient for each species was estimated from the initial slope of the data, when the $\log_{10}(E[q, \Delta])$ was plotted as a function of the Stejskal–Tanner parameter, $\gamma^2 g^2 \delta^2 (\Delta - \delta/3)$; the respective values were 3.1×10^{-10} and 6.9×10^{-10} m^2 s^{-1} for choline phosphate and water.

DMSO q-Space Plots

Figure 5 shows q-space plots from DMSO and water in a 0.60-Ht erythrocyte suspension. A notable difference in the two plots is that the DMSO curve is higher, for all q values, than the water curve. Besides this difference, it is evident that the DMSO curve is similar in overall form to that of water; the q positions of the maxima and minima are basically the same but shifted (slightly) to the left. Specifically, common q_{min} values are at $\sim 1.8 \times 10^5$, 3.7×10^5, and 5.4×10^5 m^{-1}.

It was initially anticipated that the diffusion-interference effect would also be manifest in the DMSO curve; however, it was not discernible in any of the experiments.

Simulations of q-Space Plots

Figure 6A shows the particular geometrical arrangement of model erythrocytes used for the computer simulation of NMR diffusion-coherence phenomena. The cells were assumed to occupy the centers of regular hexagonal prisms arranged with their faces in the two-dimensional crystallographic space group $p3$; and the corresponding sides were arranged as linear $p1$. Figure 6B shows two simulated erythrocytes with their axis of rotational symmetry orthogonal to $\mathbf{B}_0$.

Figure 7 shows the results of computer simulations in which the erythrocytes were assumed to occupy 50% of the sample volume, and the point water molecules were allowed to undergo random walks under four different conditions. Figure 7A shows the q-space plot for a system in which the water molecules were confined to diffuse in the intracellular compartments only and they were not allowed to undergo exchange across the membrane. Thus, there were no contributions to the signal from extracellular water. The q_{min} values were at 166,710 and 351,981 m^{-1}. The reciprocals of these values are 6.00 and 2.84 μm, respectively. The main diameter of the virtual erythrocyte was set to 8 μm; thus the scaling factors that
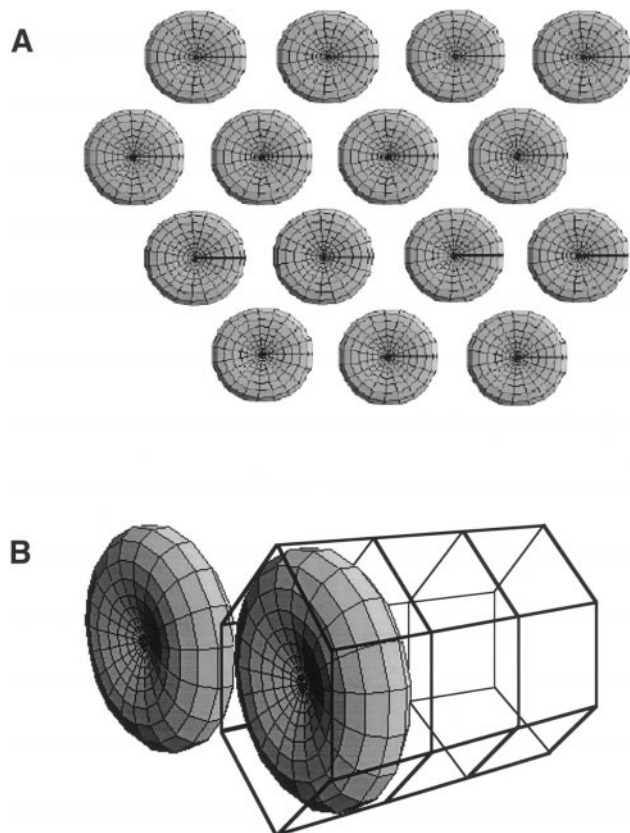

FIG. 6. (A) Schematic representation of a section of one layer of the array of discocytes used in the Monte Carlo random walk simulation of diffusion in a suspension of erythrocytes. (B) A detailed view of a discocyte and one of its neighbors in a "unit cell" in the space-filling hexagonal-prism three-dimensional tessellation, used in modeling a q-space experiment.
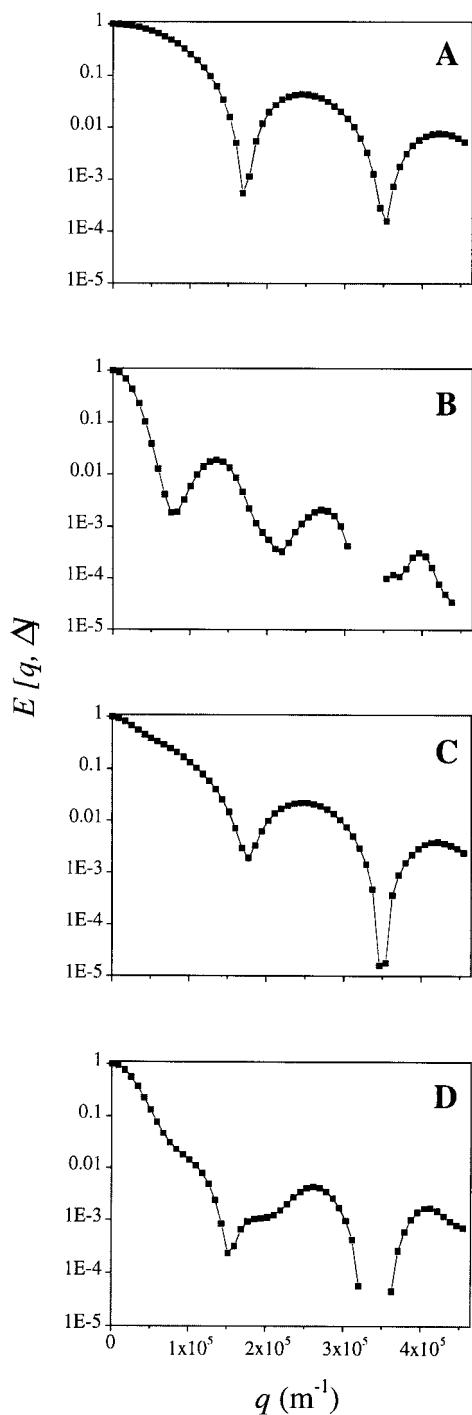
FIG. 7. Simulated q-space plots for molecules diffusing outside and inside cells, of the shape and spatial organization shown in Fig. 6. (A) Data obtained when the NMR-detected molecules were restricted exclusively to the intracellular compartment; this gave rise to the diffusion-diffraction effect in the q-space plot. (B) Simulation with the detected molecules diffusing exclusively in the extracellular region; this gave rise to the diffusion-interference effect. (The discontinuity in this curve, and the two below, was due to negative values of $E[q, \Delta]$, which can arise with the present type of finite system, and for which the logarithm is physically meaningless.) (C) Data from the situation in which the detected molecules diffused in both the intra- and extracellular regions; the curve was shown to be the sum of the two curves in A and B. (D)

relate the position of each diffusion-diffraction minimum to the main cell diameter (d) were calculated to be 1.333 and 2.82, respectively; thus $d = 1.333/q_{min,1}$ for the first minimum, and $d = 2.82/q_{min,2}$ for the second (or $d = 2 \times 1.41/q_{min,2}$).

The Bessel function relationships that describe q-space plots for diffusion in transverse cylinders and spheres are not strictly periodic (*10*). This is also the case for the model erythrocyte since the scaling factor for the second minimum was not an integral multiple of that for the first.

Figure 7B shows the coherences that arose when water was confined to diffuse in the extracellular region and was not allowed to exchange across the cell membranes. In this case the signal attenuation was much more rapid and the first minimum occurred at a much smaller q value (80,869 m^{-1}) than in Fig. 7A. However, by analogy with pore hopping around closely packed spheres of uniform size (*4*), a simple relationship exists between the main cell diameter and the position of the first two maxima. Thus $q_{max,1} = 132,904$ and $q_{max,2} = 268,460$ m^{-1} and therefore the "rules" that relate the positions of the maxima to the cell diameter are $d = 1.063/q_{max,1}$ and $d = 2 \times 1.073/q_{max,2}$, respectively.

Figure 7C shows the q-space plot obtained when water was allowed to diffuse in both the intra- and extracellular spaces, but without transmembrane exchange. This curve was directly superimposable on the one that resulted from the simple addition of the data in the two panels above it; this outcome was a useful verification of the simulation program. (Note that the data sets were weighted according to the relative volumes inside and outside the cell in its "virtual" hexagonal prism; in the case of an Ht of 0.50 the relative weighting was 1:1.) The two notable features of the q-space curve in Fig. 7C are that the first interference peak, evident in Fig. 7B, is only manifest as a poorly defined shoulder, and the diffraction minima evident in Fig. 7A are in almost identical positions in Fig.7C. This outcome indicates that at Ht = 0.5 the diffusion-diffraction signal dominates over that of diffusion interference.

Finally, Fig. 7D shows a simulated q-space plot for a system identical to that of Fig. 7C but here the membrane was "made" permeable to the water such that exchange across the membrane occurred. The probability of a point molecule crossing the membrane on encountering it, whether impacting it from

The same situation as in C but with exchange allowed across the cell membrane. Parameters used in the simulations: Erythrocytes, equation as given by (*15*); main diameter, 8.0 μm; center thickness, 1.0 μm; maximum thickness, 2.0 μm; volume and surface area calculated on the basis of the previous three values, 86 fL and 126 μm^2, respectively. Hexagonal unit cell: orientation as depicted in Fig. 6, with side length of the regular hexagon adjusted to give the requisite Ht value. Monte Carlo random walk: jump length less than 0.2 of the minimum distance between the cell surface and the wall of the prism; periodic boundary conditions applied at the hexagonal-prism walls (thus simulating an infinite array using just one unit cell and its contents); and the total number of trajectories for each simulation, 10×10^6. In D the "transition probability" of a molecule, when encountering the cell membrane, of passing through it was set to 0.01.

the outside or the inside, was set to a value (0.01) so that the intracellular mean residence lifetime for a point molecule matched that observed experimentally for human erythrocytes, at 37°C (*20*). There are three notable features: (1) there is a much greater extent of signal attenuation than for corresponding q values in Fig. 7C; (2) the diffusion-interference shoulder is better delineated; and (3) the values of $q_{min,1}$ (152,127 m^{-1}) are less than either of those in Fig. 7A (166,710 m^{-1}) or 7C (176,322 m^{-1}); this was also true, although less clearly defined, for the $q_{min,2}$ values.

DISCUSSION

General

In this investigation of q-space plots from erythrocyte suspensions several probe substances were used, namely choline, choline phosphate, and DMSO; these were used in order to discriminate between the features of diffusion interference and diffusion diffraction. Choline was entrapped in erythrocytes by hypotonic hemolysis and resealing, while choline phosphate was added to the suspensions without it entering the cells. By observing the proton signals from choline or choline phosphate in a PFGSE experiment, q-space plots showing only intracellular diffusion diffraction from choline, or the diffusion-interference effect from extracellular choline phosphate, were observed (Figs. 2 and 4, respectively). In addition, DMSO was added to erythrocyte suspensions as a control experiment (Fig. 2); DMSO enters the cell freely and therefore should show both coherence effects. However, the diffusion-interference shoulder was not "resolved" and so the plot was dominated by signal from the intracellular molecules.

Choline q-Space Plots and Intracellular Diffusion Diffraction

The hypotonic-lysis method used for rapidly incorporating choline into the cells caused marked changes in cell shape when the cells became resealed. These changes were clearly observable under the light microscope. As a result of these morphological changes it was not possible to correlate the features of the q-space plots of resealed cells (Fig. 2) with those of *fresh* erythrocytes (Fig. 1). The features of the q-space plots of choline and water shown in Fig. 2 did, however, provide important information regarding the diffusion of these two species in a cell suspension. First, signal attenuation at a given q value was considerably less for choline than for water. In free solution it would be expected that the water signal would be attenuated more rapidly than that of choline because water, being a smaller molecule, has a higher diffusion coefficient. In the case of restricted diffusion, differences in the rate of diffusion will not result in significantly different extents of attenuation as long as the condition $\Delta \gg a^2/2D$ (where a is the effective cell diameter) is maintained for both species. In the experiment this condition was maintained, but while cho-

line was restricted to diffuse solely within the intracellular compartments water was free to exchange across the membranes and hence to diffuse larger distances in the time Δ. The greater attenuation of the water signal can therefore be interpreted as being due, in part, to the larger mean diffusion distance available to it. A second contributing factor is that water in the extracellular region diffuses in a less viscous medium so its "intrinsic" as well as its "apparent" diffusion coefficient will be greater than that for either water or choline inside the cells.

Another significant difference in the water and choline q-space plots in Fig. 2 was the positions of the diffusion-diffraction peaks. This difference was very important because it enabled discrimination between the extracellular diffusion-interference and the intracellular diffusion-diffraction phenomena, which was the main aim of the investigation. The peak maximum at $\sim 2.0 \times 10^5$ m^{-1} in the water curve was clearly absent in the choline curve. Thus the first peak (shoulder) present in the water curve was able to be assigned to an effect of water diffusing in the space between the cells, namely "pore hopping." In other words, the phenomenon occurs only with molecules that diffuse outside the cells. By the same reasoning, the peak ($q_{max,1}$, in Fig. 2) which appears in the choline curve at $\sim 3.5 \times 10^5$ m^{-1} was readily ascribed to intracellular diffusion diffraction. Therefore, this experiment discriminated between the diffusion-interference and diffusion-diffraction effects in the q-space plots.

Diffusion-diffraction patterns in q-space plots, where rapid transmembrane exchange is present, should lead to estimates of apparent cell dimensions that are smaller than if exchange were not present (*14*). Therefore, q_{min} values for water were expected to be lower in comparison with those for choline. However, under the conditions used for Fig. 2 this was not readily discernible. Since only intracellular diffusion diffraction was manifest in the choline curve, the peak minimum ($q_{min,1}$ in Fig. 2) at $\sim 2.8 \times 10^5$ m^{-1} should be considered the "relevant" $q_{min,1}$ and not the ambiguous one for water located at $\sim 3.4 \times 10^5$ m^{-1}. The interpretation of this result is that the first interference peak for water (see Fig. 7B) is partly superimposed on the first diffraction "valley" (see Fig. 7A), thus displacing the position of the overall minimum. At first sight this displacement might be expected to be to the right, but rapid transmembrane exchange suppresses the interference effect and displaces the first (and subsequent) minimum in the overall q-space curve to the *left*. Comparing Figs. 7C and D readily demonstrates this outcome.

In a previous study (*2*) the spherical cell diameter was calculated to be $1/2.0 \times 10^5$ m^{-1} = 5.0 μm, based on the pore hopping interpretation for water diffusion outside the cells, and $1.46/3.2 \times 10^5$ m^{-1} = 4.6 μm based on the $q_{min,1}^d$ of the intracellular diffraction peak. The cell diameter estimated from $q_{min,1}$ of the choline curve was $1.46/2.8 \times 10^5$ m^{-1} = 5.2 μm, which was significantly different from the corresponding value (4.6 μm) derived from the water curve. The basis of this

difference lies in the matters discussed in the previous paragraph.

These results clearly show that the presence of both diffusion-interference and diffusion-diffraction peaks can potentially complicate the inference of compartment sizes from q-space plots of water if the first diffraction and interference peaks are used. A more accurate estimate of cell diameter comes about if the diffusion-interference effect is minimized and this can be achieved by using a high hematocrit. Alternatively, if the signal-to-noise is sufficiently high the higher order diffraction peaks (and minima) can be used as then the interference pattern makes an insignificant contribution to the overall q-space signal. The remaining complication to the interpretation of the data is the extent to which the transmembrane exchange causes a shift in the diffraction minima. The extent of this effect can be judged from the data in Fig. 5.

Choline Phosphate and Extracellular Diffusion Interference

It is instructive to compare the curve for choline phosphate in Fig. 4 with that for choline in Fig 2: the choline phosphate signal declines more steeply, over the first few q values up to 2.0×10^5 m^{-1}. However, choline phosphate, being a larger molecule, has a smaller intrinsic diffusion coefficient than choline, so the greater signal attenuation of choline phosphate cannot be ascribed to a larger intrinsic diffusion coefficient. The proposed reason for the more rapid attenuation of the signal is that the motion of choline phosphate is less restricted, as a result of it only being in the extracellular space.

It can also be seen in Fig. 4 that $q_{max,1}$ for choline phosphate (upper curve) and $q_{max,1}$ for water (lower curve) do not coincide. Specifically, there are two major coherence peaks in the choline phosphate plot that are centered at $\sim 1.5 \times 10^5$ m^{-1} ($q_{max,1}$) and $\sim 2.6 \times 10^5$ m^{-1} ($q_{max,2}$), while for water there is a shoulder at $\sim 1.2 \times 10^5$ m^{-1} and a peak at $\sim 2.3 \times 10^5$ m^{-1}. Since the choline phosphate molecules were confined to the outside of the cells, the two maxima can be ascribed only to the diffusion-interference phenomenon. The position of the water peaks at a lower value of q can be attributed to the fact that water exchanges between the inside and the outside of the cells (1, 14). In effect this makes the available mean diffusion distance of the outside water larger because of access to the inside of the cells. The effect is well illustrated by comparing the q position of the first peak in Fig. 7B and the shoulder in Fig, 7D.

The diffusion-interference peak at $\sim 1.2 \times 10^5$ m^{-1} (shoulder, $q_{max,1}$ in Figs. 1 and 4) was not evident with high hematocrit samples of discocytes. This is in contrast with the shoulder seen with *spherical* erythrocytes where it was *pronounced* (see Figs 2 and 3).

In Fig. 4 the shoulder on the water curve, to a first approximation, implies a cell diameter of 8.3 μm; this value was arrived at by assuming that the cells approximate flat cylinders with their axis of rotational symmetry orthogonal to $\mathbf{B}_0$ and for this arrangement the diameter is given by $1.23/q_{max,1}$ (1, 2). By

the same reasoning, the first choline phosphate peak corresponds to a mean cell diameter of 6.7 μm. The difference between the two values is, again, ascribable to the effect of the transmembrane exchange of water (1, 14). This matter is discussed next.

DMSO q-Space Plots

In Fig. 5 the close similarity of the forms of the q-space plots from DMSO and water, and the fact that DMSO is known to permeate the cell membrane, suggests that the DMSO coherences also arise from the same phenomena as for water. However, DMSO permeation through cell membranes is slow on the NMR time scale so it would be expected that the diffusion-diffraction minima would be at (slightly) smaller values of q, and this is indeed evident in Fig. 5. The differences in q_{min} values give an indication of the possible magnitude of errors in estimates of mean cell diameter when the probe molecule is in rapid exchange across the cell membranes. The positions of the second- and third-order diffusion-diffraction peaks are much less affected by underlying diffusion-interference peaks (see Fig. 7 and discussion below) so a comparison of the $q_{min,2}$ and $q_{min,3}$ values (notwithstanding lower signal-to-noise) would give a more accurate impression of the effects of transmembrane exchange on estimates of cell diameter.

The q-space plot of the DMSO data in Fig. 5 is similar to the simulated data in Fig. 7C while the water data are more like the simulated data in Fig. 7D; this is consistent with the relative rates of transmembrane exchange of the two molecules. Furthermore it is clear from Fig. 7C that if there is no (or slow) transmembrane exchange that the first diffusion-interference peak is much less well defined and this is seen with the DMSO data in Fig. 5.

Simulations of Cellular System Showing Diffusion Coherence

In order to check the physical interpretations of the features of the q-space plots, numerical simulations of diffusion, modeled as a three-dimensional random walk in an array of semipermeable discocytes (Fig. 6), were shown to be valuable (Fig. 7). The ability to modulate transmembrane exchange between completely "on" and completely "off" states enabled the independent study of the diffraction and interference effects. Where point molecules were confined exclusively to the extracellular region the effects were able to be identified as interference effects. When point molecules were confined exclusively to the intracellular region the effects could be assigned to diffusion diffraction. When exchange was turned on the combined effects of diffusion interference and diffusion diffraction were observed. Therefore, in all cases the features of the q-space plots could be related to the main cell diameter.

It is also worth noting that the signal from the diffusion-interference phenomenon was substantially weaker than that from diffusion diffraction. Therefore, when both phenomena were in operation the combined q-space curve was dominated

by the latter (Figs. 7A and 7B), and this result is consistent with the experimental results (Figs. 1, 4, and 5).

The simple scalar relationships between the values of q_{max} and cell diameter, in the diffusion-interference data, only apply at higher packing densities of the cells, around Ht = 0.50 (Fig. 7B). (However, at Ht values above ~ 0.7 the small fraction of extracellular water implies a smaller interference signal.) By analogy, in a bed of randomly packed spheres of equal diameter, the pores are separated by a mean distance that is closely approximated by the diameter of a sphere (10). However, if the spheres are dispersed (and stay suspended by "density matching" with the solvent) then clearly the distances between the centers of the pores will be greater than the diameter of the spheres. Thus in q-space analysis, the position of q_{max} does not correspond simply to the reciprocal of the sphere diameter for dilute suspensions; the same would be true for erythrocytes in a dilute suspension. In addition, it is expected that the packing geometry will impact upon the features of q-space plots from arrays of cells; the extent of this variation warrants further study.

CONCLUSIONS

Since the q-space plots of water in erythrocyte suspensions display both intracellular and extracellular coherences, while the choline curve (Fig. 2) shows only intracellular diffraction, it can be concluded that the presence of the interference peak in the water curve partially obscures its diffraction coherence(s) (compare Figs. 7A and 7B). It was expected that the water curve would also display a peak at $q_{max} \sim 3.5 \times 10^5$ m^{-1} as was the case with choline (Fig. 2, upper curve), but this was absent. This absence is concluded to have been caused by the dominant overlapping diffraction peak (see Fig. 7C). Also, there was a minimum in the choline curve (Fig. 2) at $\sim 2.8 \times 10^5$ m^{-1} which was not present in the water curve. This difference can be attributed to the presence of its interference peak at $q \sim 1.8 \times 10^5$ m^{-1}. The minimum in the water curve at $q_{min,1} \sim 2.8 \times 10^5$ m^{-1} was therefore concluded to have been caused by diffusion interference since it was absent in the case of choline which only gave diffusion-diffraction effects.

Factors that affect the distinctness of the features of q-space plots have been considered in earlier work on "artificial" (12, 13) and cellular systems (2). In the case of cell suspensions, the diffraction effects are also "blurred" by heterogeneity of cell shapes and sizes (2, 3). For cells such as erythrocytes, which have only one axis of rotational symmetry, orientation with their axis orthogonal to $\mathbf{B}_0$ clearly creates a favorable situation for observing diffusion-coherence effects (1, 2), as also reported herein. Physical and chemical (metabolic) factors that affect the uniformity of this orientation across the entire cell population will also degrade the distinctness of the coherence patterns.

Finally, assignment of the features of q-space plots from erythrocyte suspensions by direct experimental means and consistency of Monte Carlo simulations with inferences drawn from these data pave the way for more quantitative interpretations of such data from other forms of erythrocytes, and more complex cell types and arrays.

ACKNOWLEDGMENTS

REFERENCES

1. P. W. Kuchel, A. Coy, and P. Stilbs, *Magn. Reson. Med.* **37,** 637 (1997).

2. A. M. Torres, R. J. Michniewicz, B. E. Chapman, G. A. R. Young, and P. W. Kuchel, *Magn. Reson. Imaging* **16,** 423 (1998).

3. D. Cory and A. N. Garroway, *Magn. Reson. Med.* **14,** 435 (1990).

4. P. T. Callaghan, A. Coy, D. Macgowan, K. J. Packer, and F. O. Zelaya, *Nature* **351,** 467 (1991).

5. P. T. Callaghan, A. Coy, T. P. J. Halpin, D. Macgowan, K. J. Packer, and F. O. Zelaya, *J. Chem. Phys.* **97,** 651 (1992).

6. P. P. Mitra and P. N. Sen, *Phys. Rev. B* **45,** 143 (1992).

7. A. J. Lennon, "A Pulsed Field Gradient NMR and Random-Walk Simulation Study of Diffusion in Heterogeneous Systems," Ph.D. dissertation, Department of Biochemistry, University of Sydney (1995).

8. F. A. Jenkins and H. E. White, "Fundamentals of Optics," 3rd Ed., McGraw–Hill, New York (1957).

9. P. T. Callaghan, "Principles of Magnetic Resonance Microscopy," Oxford Univ. Press, Oxford (1991).

10. P. T. Callaghan, *J. Magn. Reson. A* **113,** 53 (1995).

11. P. T. Callaghan, *Magn. Reson. Imaging* **14,** 701 (1995).

12. P. T Callaghan and A. Coy, *in* "Nuclear Magnetic Resonance Probes of Molecular Dynamics" (R. Tycko, Ed.), Kluwer, Amsterdam (1994).

13. M. Appel, G. Fleischer, D. Geschke, J. Kärger, and M. Winkler, *J. Magn. Reson. A* **122,** 248 (1996).

14. A. V. Barzykin, K. Hayamizu, W. S. Price, and M. Tachiya, *J. Magn. Reson. A* **114,** 39 (1995).

15. P. W. Kuchel and E. D. Fackerell, *Bull. Math. Biol.,* in press (1999).

16. G. R. Beilharz, C. R. Middlehurst, P. W. Kuchel, G. E. Hunt, and G. F. S. Johnson, *Aust. J. Exp. Biol. Med. Sci.* **64,** 271 (1986).

17. A. J. Lennon and P. W. Kuchel, *J. Magn. Reson. A* **111,** 208 (1994).

18. S. Wolfram, "The Mathematica Book," Version 3, Cambridge Univ. Press, Cambridge (1996).

19. A. J. Lennon and P. W. Kuchel, *J. Magn. Reson. A* **107,** 229 (1994).

20. Gh. Benga, V. I. Pop, O. Popescu, and V. Borza, *J. Biochem. Biophys. Methods* **21,** 87 (1990).